A MATTER–ANTIMATTER UNIVERSE?

A.G. Cohen[a], A. De Rújula[b,a] and S.L. Glashow[c,a] *

[a]*Department of Physics, Boston University, Boston, MA 02215, USA*
[b]*Theory Division, CERN, 1211 Geneva 23, CH*
[c]*Lyman Laboratory of Physics, Harvard University, Cambridge, MA 02138, USA*

Abstract

We ask whether the universe can be a patchwork consisting of distinct regions of matter and antimatter. We demonstrate that, after recombination, it is impossible to avoid annihilation near regional boundaries. We study the dynamics of this process to estimate two of its signatures: a contribution to the cosmic diffuse γ-ray background and a distortion of the cosmic microwave background. The former signal exceeds observational limits unless the matter domain we inhabit is virtually the entire visible universe. On general grounds, we conclude that a matter–antimatter symmetric universe is empirically excluded.

1   Introduction and Outlook

The laws of physics treat matter and antimatter almost symmetrically, and yet the stars, dust and gas in our celestial neighborhood consist exclusively of matter. The absence of annihilation radiation from the Virgo cluster shows that little antimatter is to be found within ~ 20 Mpc, the typical size of galactic clusters. Furthermore, its absence from X-ray-emitting clusters implies that these structures do not contain significant admixtures of matter and antimatter.

---

*cohen@bu.edu, derujula@nxth21.cern.ch, glashow@physics.harvard.edu

Many cosmologists assume that the local dominance of matter over anti-matter persists throughout the entire visible universe. A vast literature attempts to compute the baryonic asymmetry from first principles. However, observational evidence for a *universal* baryon asymmetry is weak. In this regard, searches for antimatter in cosmic radiation have been proposed [1]–[3]. Early next century, the AntiMatter Spectrometer (AMS), deployed aboard the International Space Station Alpha [2, 3], will search for antimatter in space. Its reach is claimed to exceed 150 Mpc [4]. The detection of cosmic anti-alpha particles would indicate the existence of primordial antimatter; the detection of anti-nuclei with $Z > 2$ would imply the existence of extra-galactic anti-stars.

The possible existence of distant deposits of cosmic antimatter has been studied before [5]–[8]. Steigman [5] concluded that observations exclude significant matter–antimatter admixtures in objects ranging in size from planets to galactic clusters. Stecker *et al.* [6] interpreted an alleged shoulder in the cosmic diffuse gamma (CDG) spectrum near 1 MeV[1] as relic γ-rays from antimatter annihilation. Recently, Dudarewicz and Wolfendale [8] used similar arguments to reach a contrary conclusion: that the observed CDG spectrum rules out any large antimatter domains. These conflicting results are not based on specific dynamics in a consistent cosmology. Our analysis uses current data and avoids *ad hoc* assumptions concerning a matter–antimatter universe.

We explore the possibility of universal (but not local) matter-antimatter symmetry. In what we term the $B = 0$ universe, space is divided into regions populated exclusively by matter or antimatter. Our conclusions do not depend on how this structure evolved, but it is reassuring to have an explicit model in mind: consider an inflationary cosmology in which baryon (or antibaryon) excesses develop in the manner suggested by Sakharov [9]. In models with spontaneous CP violation, the Lagrangian may be chosen judiciously so that the 'sign' of CP violation (determining whether a local baryon or antibaryon excess develops) is randomly and abruptly assigned to regions as they emerge from their horizons during inflation. Soon after baryogenesis, the domain walls separating matter and antimatter evaporate. As regions of matter or antimatter later re-enter their horizons, the $B = 0$

---

[1]We refer to cosmic diffuse photons by conventional names according to the current photon energy: the night sky, the CDG and the CBR refer to visible, ~ 1 MeV and microwave photons, respectively.

universe becomes a two-phase distribution.

Let today's domains be characterized by a size d_0, such that $1/d_0$ is their mean surface-to-volume ratio. Because the existence of anti-galaxies within a matter-dominated domain is empirically excluded, we must (and can) arrange the distribution of domains to be sharply cut off at sizes smaller than d_0. Explicit inflationary models satisfying these constraints exist [10], but are described no further because we find all such models to conflict with observation.

The current domain size d_0 is the only parameter of the $B = 0$ universe crucial to the confrontation of theory with observation. To agree with constraints from X-ray-emitting clusters, d_0 must exceed a minimal value, ~ 20 Mpc. For $d_0 = 20$ Mpc, the visible universe would consist of $\sim 10^7$ domains. We derive a stronger lower limit on d_0 comparable to the current size of the visible universe, thereby excluding the $B = 0$ universe.

An explicit cosmological model is necessary to estimate the observable signals produced by annihilation. We assume a Robertson–Walker universe and use fiducial values for the relevant cosmological parameters: critical mass density $\Omega = 1$; vanishing cosmological constant $\Omega_\Lambda = 0$; Hubble constant $H_0 = 75$ km/s·Mpc or $h = 0.75$; and an average baryon (or antibaryon) number density $n_B \equiv \eta\, n_\gamma$ with $\eta = 2 \times 10^{-10}$.

In Section 6 we show that our conclusions are unaffected by other choices for Ω, Ω_Λ and H_0 within their empirically allowed domains. Consequently we do not express our results explicitly in terms of these cosmological parameters. The annihilation signals we study depend linearly on η. To compute lower limits to the signals, we chose η at the low end of the domain allowed by analyses of primordial element abundances. (For a recent discussion, see [11].)

In Section 2 we explain why particle–antiparticle annihilation is unavoidable from the time of recombination to the onset of structure formation. Following a conservative approach, we consider only those annihilations occurring during this period. Our analysis involves known principles of particle, atomic and plasma physics, but the dynamics of the annihilating fluids (discussed in Section 3) is complicated and the considerations required to reach our results are elaborate.

The immediate products of nuclear annihilation are primarily pions (π^+, π^0 and π^-) with similar multiplicities and energy spectra. The end products

3

are energetic photons from π^0 decay, energetic electrons[2] (e^+ and e^-) from the decay chain $\pi \rightarrow \mu \rightarrow e$, and neutrinos. Although they are produced at cosmological distances, the annihilation photons and electrons can each produce potentially observable signals:

- The energy carried off by annihilation electrons (about 320 MeV per annihilation) affects the CBR spectrum directly (via Compton scattering) and indirectly (by heating the medium). The consequent distortion of the CBR (discussed in Section 4) cannot exceed observational limits.

- Most of the annihilation photons, although redshifted, are still present in the universe. Their flux (computed in Section 5) cannot exceed the observed CDG flux.

Because these signals increase inversely with the domain size, our analysis yields a lower limit for d_0. In fact, we obtain no new constraint from comparing the expected distortion of the CBR with its measured limits. However, the CDG flux produced by annihilation far exceeds the observed flux unless d_0 is comparable in size to the visible universe. Thus, the $B = 0$ universe is excluded.

2   The Era of Unavoidable Annihilation

What if the matter and antimatter domains are and have always been spatially separated? If large empty voids lay between them, there would be no observable annihilation signals. We now show how the observed uniformity of the CBR rules voids out.

Two events took place at roughly the same time in cosmic history: the transition from charged plasma to neutral atoms (recombination) and the decoupling of radiation and ordinary matter (last scattering). For our fiducial cosmological parameters, these events occurred at a temperature ~ 0.25 eV and at a redshift $y_R \simeq 1100$ (we use $y \equiv 1 + z = 1/R(t)$ as a redshift parameter, rather than the conventional z). The transition to transparency was not instantaneous, but evolved during an interval $y_R \pm 100$ whose half-width is ~ 15 Mpc in comoving (current) distance units. Thus, features at recombination of comoving size smaller than 15 Mpc cannot be discerned in the CBR.

---

[2]Relativistic electrons and positrons behave similarly, and we refer to both as electrons.

Large-scale non-uniformities of the matter density, whether dark or baryonic [12] generate variations of the CBR temperature. Its observed uniformity (to parts in 10^{-5}) implies a very uniform density of ordinary matter at $y = y_R \simeq 1100$, to within the resolution discussed above. It follows that voids between matter and antimatter domains must be smaller than 15 Mpc.

The baryon density depletion in voids is damped as photons diffuse toward less dense regions, dragging matter with them. By recombination, inhomogeneities with current size $\lesssim 16$ Mpc would be destroyed[3] by this mechanism [13]. This upper bound coincides with the smallest resolvable structure in the CBR. Thus, voids large enough to survive until recombination would have been detected. While matter and antimatter regions may have been separated prior to recombination, they must be in immediate contact afterward. Thus, in determining the minimal signal of a $B = 0$ universe, we do not consider annihilations occurring at $y > y_R$.

The mechanism by which the nearly uniform universe at large y evolved today's large-scale structures is not well understood. We cannot confidently assert what effects this will have on annihilation in a $B = 0$ universe. It could well be that the collapse of baryonic matter into galaxies and stars quenches annihilation unless the collapsing system overlaps a domain boundary, a situation we consider shortly. Our conservative estimate of the annihilation signal includes matter–antimatter annihilation taking place prior to the redshift y_S at which the earliest density fluctuations become large ($\delta\rho/\rho \sim 1$). We take $y_S \simeq 20$, which is estimated to be the epoch of galactic condensation [14] and earliest star formation [15]. We compute the signals due to annihilations taking place during the interval $1100 > y > 20$.

The large-scale density contrast of the visible universe need not coincide with the pattern of matter and antimatter domains. A density fluctuation beginning to collapse could overlap a domain boundary. Successful collapse would yield a structure with a significant mixture of matter and antimatter. In this case annihilation would proceed even more rapidly at the onset of structure formation. Yet we cannot be confident that such mixed structures form.

In the linear regime ($\delta\rho/\rho \ll 1$), the mean annihilation rate is not affected by density fluctuations. But, what happens as the fluctuations grow? If an over-density is to overcome expansion and become a self-gravitating

---

[3]This assumes that such inhomogeneities are not strictly isothermal, a situation considered in Section 6.

system, it must satisfy the Jeans condition: the sound travel time across the object l/v_s must be greater than the characteristic free-fall time $1/\sqrt{G\rho}$, or $G\,l^2\rho \geq v_s^2$. Suppose that equality is approached by an over-density containing both matter and antimatter. Further contraction increases the annihilation rate, thus reducing ρ and driving the system away from collapse. Thus, our conservative estimate of the annihilation signal assumes that density fluctuations straddling domain boundaries either fail to collapse or form separate unmixed structures.

3 The Matter–Antimatter Encounter

The $B = 0$ universe consists of matter and antimatter domains with almost identical mass densities that, as we have shown, touch one another from recombination to the onset of structure formation. As annihilation proceeds near an interface, a flow develops as new fluid replenishes what is annihilated. This flow must be analyzed to determine the annihilation rate on which our putative signals depend. The analysis involves established and well-understood principles of physics, but is complicated by the energy released by nuclear annihilation. (We neglect e^+e^- annihilation, whose energy release is much smaller.) The processes by which annihilation electrons lose energy produce crucial effects on the ambient fluid, as well as a potentially observable distortion of the CBR. (High-energy photons from π^0 decay, although responsible for the CDG signal, have little effect on the medium through which they pass.)

The primary energy-loss mechanism of the annihilation electrons is Compton scattering off CBR photons (see Appendix A). This process up-scatters target photons to higher energies. The resultant flux of UV photons heats and ionizes ambient matter throughout much of the universe and for all of the relevant period. Moreover, the annihilation electrons lose a small portion of their initial energies by scattering off ambient electrons in the fluid. This process heats the fluid within the electron range, thereby accelerating the flow and leading to even more annihilation—a feedback mechanism making the matter–antimatter encounter potentially explosive.

Several length scales characterize the fluid dynamics about a matter–antimatter interface. They are:

- A, the width of the *annihilation zone,* wherein both matter and antimatter are present;

- D, the width of the *depletion zone,* wherein fluid flow toward the annihilation zone reduces the density;

- L, the width of the *reheated zone,* wherein electrons produced by annihilations directly deposit energy into the fluid. This is simply the electron range.

These length scales, computed in Appendix A.1 and later in this section, are shown in Fig. 1 along with a comoving domain size of 20 Mpc and the horizon scale. Annihilation takes place in the vicinity of the domain boundary and well within the depletion zone, which itself is much shorter than the electron range. That is, in the relevant redshift domain: $A \ll D \ll L$. This distance hierarchy lets us treat the flow as one-dimensional.

Annihilation has a negligible effect on the CBR temperature $T_\gamma(y)$, which remains as it is in a conventional universe. However, the annihilation debris produce and maintain virtually total ionization, as shown in Appendix A.3. Therefore the annihilating fluid consists of photons, protons, antiprotons, electrons and positrons[4]. The proton and electron number densities coincide, except in the narrow annihilation zone. Consequently our analysis may be put in terms of the total matter mass density $\rho \equiv m_e n_e + m_p n_p$, the total fluid momentum density ρv, the total fluid pressure p and the total fluid energy density $\epsilon = \epsilon_{\text{thermal}} + \rho v^2/2$. The internal energy density and pressure are related as for a non-relativistic ideal gas: $\epsilon_{\text{thermal}} = 3\,p/2$.

The equations describing the flow of matter are conservation laws for particle number (mass in the non-relativistic limit), momentum, and energy. They must take account of the following phenomena:

- The depletion of fluid mass, momentum and energy by nuclear annihilation.

- The effect of the CBR on the fluid momentum and energy.

- The effect of the annihilation products on the fluid momentum and energy.

- The expansion of the universe.

---

[4]We neglect the helium contamination ($\sim 7\,\%$ by number) and those of larger primordial nuclei.
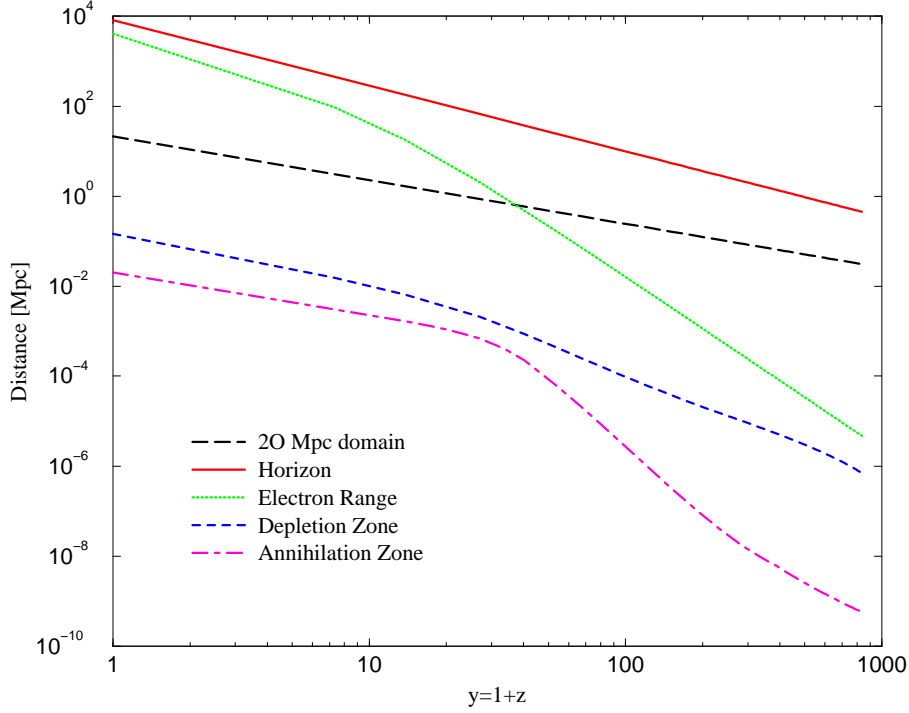
Figure 1: Read from the top at large y: the horizon, the look-back size of a 20 Mpc domain, the widths of the reheated zone, the depletion zone, and the annihilation zone.

The expansion of the universe is taken into account by expressing the conservation laws in a Roberston–Walker universe [16]. The metric is $ds^2 = dt^2 - R^2(t)d\chi^2$, with χ a comoving spatial coordinate normal to a domain boundary. The remaining effects are dealt with by including appropriate source terms in the fluid equations:

$$\frac{\partial \rho}{\partial t} + 3\frac{\dot{R}}{R}\rho + \frac{1}{R}\frac{\partial(\rho v)}{\partial \chi} = -\Gamma_{\text{ann}}\,\rho \tag{1}$$

$$\frac{\partial(\rho v)}{\partial t} + 4\frac{\dot{R}}{R}\rho v + \frac{1}{R}\frac{\partial}{\partial \chi}[\rho v^2 + p] = -\Gamma_{\text{ann}}\,\rho v - \frac{4}{3}\sigma_T\frac{u_\gamma}{m_p c}\rho v \tag{2}$$

$$\frac{\partial \epsilon}{\partial t} + 5\frac{\dot{R}}{R}\epsilon + \frac{1}{R}\frac{\partial}{\partial \chi}[(\epsilon + p)v] = -\Gamma_{\mathrm{ann}}\epsilon - \frac{4}{3}\sigma_T \frac{u_\gamma}{m_e c}\left(\frac{3\,p}{2} - \frac{3\,\rho\,T_\gamma}{m_p}\right) + H_\epsilon \;. \quad (3)$$

Here $\Gamma_{\mathrm{ann}} \equiv \langle\sigma_{\mathrm{ann}}v\rangle\bar{n}_p$ is the matter annihilation rate, σ_T is the Thompson cross section and u_γ is the CBR energy density. The terms involving σ_T describe the transfer of energy and momentum between the fluid and the CBR resulting from Compton scattering. H_ϵ, given by Eq. (31) in Appendix A, is the rate of change of the energy density of the fluid due to its interactions with the annihilation debris. It receives a direct contribution from the annihilation electrons, and an indirect one from UV photons up-scattered by Compton collisions of these electrons with the CBR. We find that the contribution of the electrons dominates within the electron range. Beyond this range, only the UV photons contribute to H_ϵ. In Eq. (2), we have neglected the small contribution by the annihilation debris to the fluid momentum.

The signals of a $B = 0$ universe—the CDG and a distortion of the CBR—are functions of J, the number of annihilations taking place per unit time and area orthogonal to the surface of an annihilation zone:

$$J \equiv \int \langle\sigma_{\mathrm{ann}}v_{p\bar{p}}\rangle\, n_p\bar{n}_p\, R\, d\chi \;, \quad (4)$$

where the integral extends over a single annihilation zone with $\chi = 0$ at its mid-point, and $\bar{n}_p(\chi) = n_p(-\chi)$. The width of the annihilation zone A may be estimated as $A \sim J/\langle\sigma_{p\bar{p}}v\rangle n_\infty^2$, where [17] $\sigma_{p\bar{p}}v \simeq 6.5 \times 10^{-17}$ cm^3 s^{-1} c/v and n_∞ is the proton density far from the annihilation zone. We must solve Eqs. (1–3) to determine J.

3.1 A Qualitative Solution

Because our fluid equations do not admit analytic solutions we begin with a qualitative discussion. The value of Γ_{ann} is always much greater than the expansion rate, so that the solutions to Eqs. (1)–(3) rapidly reach equilibrium in the annihilation zone. Consequently, taking the limit $\sigma_{\mathrm{ann}} \to \infty$ yields a good approximation. In this limit, the width of the annihilation zone shrinks to zero and the annihilation terms in the fluid equations may be replaced by a boundary condition at the domain interface. The rate of annihilation per unit surface area is then given by the proton flux at the interface:

$$J \simeq \frac{\rho(\chi,t)}{m_p}\, v(\chi,t)\bigg|_{\chi=0} \;. \quad (5)$$

Two effects result from the couplings of the fluid to the CBR. The term in Eq. (2) proportional to σ_T tends to damp the fluid motion. The corresponding term in Eq. (3) tends to keep the fluid temperature near T_γ. For $y \gtrsim 400$ these terms dominate, so that the two temperatures are locked together, $T \simeq T_\gamma$. The CBR drag on the fluid leads to diffusive motion, and we may define a time-dependent diffusion constant:

$$D_{e\gamma} \equiv \frac{45}{4\,\pi^2\,\sigma_T\,T_\gamma^3}\,. \tag{6}$$

The solution to the resulting diffusion-like equations gives an estimate of the annihilation rate J:

$$J \simeq n_\infty(t)\,\sqrt{\frac{5\,D_{e\gamma}}{3\,\pi\,t}} \tag{7}$$

with n_∞ the proton number density far from the interface. The width of the depletion zone is comparable to the diffusion length $D \sim \sqrt{D_{e\gamma}\,t}$.

For redshifts $y \lesssim 200$ the effects of the CBR on the fluid motion are negligible and we may ignore terms proportional to σ_T. In this case, which we refer to as 'hydrodynamic', the motion is controlled by pressure gradients and the fluid flows at a substantial fraction of the speed of sound. The resulting equations are those describing a gas expanding into a semi-infinite vacuum in the presence of an energy source. An analytic solution exists for $H_\epsilon = 0$. In this case the annihilation rate J is

$$J = C\,n_\infty(t)\,v_\infty(t) = C\,n_\infty(t)\,\sqrt{\frac{5\,T_\infty(t)}{3\,m_p}} \tag{8}$$

with v_∞ the speed of sound and T_∞ the fluid temperature $T = p/(n_p + n_e)$ far from the annihilation zone. The coefficient of proportionality is[5] $C = (3/4)^4$. The width of the depletion zone in this case is comparable to the sound-travel distance $D \sim R(t)\int^t dt'\,v_\infty/R$.

In the intermediate region, $200 \lesssim y \lesssim 400$, neither of the above approximations give a quantitatively accurate picture of the fluid motion.

---

[5]This is the adiabatic solution. For $100 \lesssim y \lesssim 200$ the process is more nearly isothermal. The corresponding value of C is $1/e$.

3.2 The Numerical Solution

We have integrated Eqs. (1–3) numerically to determine the fluid temperature T and the annihilation rate per unit surface area J near a domain boundary. The diffusive nature of the solution at large y has a welcome consequence: all memory of the initial conditions is lost as the fluid evolves. The post-recombination annihilation signal does not depend on the (pre-recombination) time at which matter and antimatter domains first come into contact. To solve Eqs. (1)–(3) we choose initial conditions at recombination such that the matter and antimatter domains have constant density, have no peculiar velocity and touch along the surface $\chi = 0$. Our results are more conveniently presented in terms of y rather than time, according to $dy = -y\,H(y)\,dt$. For our fiducial choice of cosmological parameters $H(y) = H_0\,y^{3/2}$.

The dotted curve in Fig. 2 is the fluid temperature $T(y)$ in a conventional universe. The remaining two curves are the computed temperatures of the $B = 0$ universe: the solid curve is $T(y)$ within the electron range where heating by relativistic electrons dominates; the dashed curve is its value outside this region, where UV photons are the only heat source. For $y \gtrsim 400$, the CBR is an effective heat bath keeping matter and radiation close to thermal equilibrium. Heating due to the annihilation products plays an important role at lower y: it increases the fluid temperature leading to a larger fluid velocity. According to Eq. (5) the annihilation rate J is thereby enhanced.

The solid curve in Fig. 3 is our numerical result for J, the annihilation rate per unit surface area defined by Eq. (4). The dashed curve is the approximation given by Eq. (8) using the temperature obtained from the numerical integration. Although its derivation ignored H_ϵ, Eq. (8) agrees quite well with our numerical result for this choice of $T(y)$. At larger redshifts, the motion is diffusive and our numerical result should be (and is) substantially less than the qualitative hydrodynamic estimate[6], as is seen in the figure. Had we used the matter temperature of a conventional universe in Eq. (8), we would have obtained an annihilation rate nearly two orders of magnitude smaller. The heating of the fluid by annihilation debris (described by H_ϵ) has a dramatic effect on the annihilation rate J, and *a fortiori* on the consequent signals of the $B = 0$ universe.

At all redshifts the annihilation rate is determined by the flow of the

---

[6]Our diffusive results for $y \gtrsim 400$ are at variance with those of [18], where the annihilation rate prior to recombination is estimated on the basis of proton free-streaming.
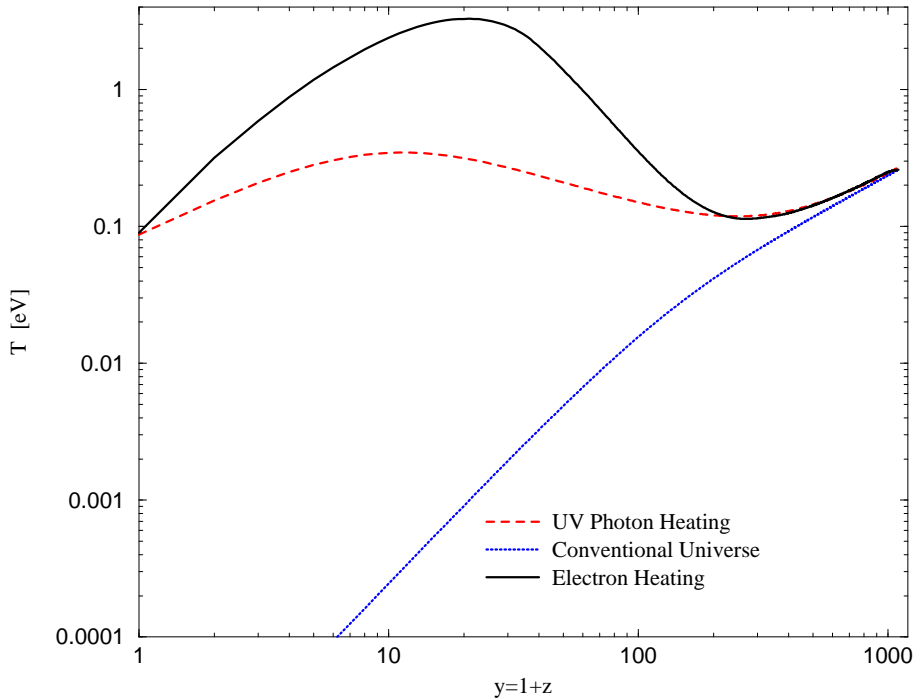
Figure 2: Temperatures (in eV) as functions of redshift $y \equiv 1 + z$.

highly ionized matter and antimatter fluids into the annihilation zone. The momentum-transfer cross section σ_C in proton-antiproton Coulomb collisions, which controls diffusive mixing of these fluids, is large compared to the annihilation cross section σ_{ann}. If mixing results only from diffusion, as in quasi-static laminar flow, the annihilation current would be reduced by a factor $\sim (\sigma_{\mathrm{ann}}/\sigma_C)^{1/2}$ relative to J. However turbulence produces full mixing in the annihilation zone, while leaving the average flow unaffected, thus justifying our neglect of the Coulomb scattering term in equations (1–3).

An analysis of fluctuations about a laminar flow into the annihilation zone demonstrates an instability towards turbulent mixing (this is analogous to the instability of a planar flame front in combustive flow [19].) For the width A of the annihilation zone we have obtained, the Reynolds number is $\mathcal{R}_A \sim A\,\sigma_C\,n > 10^5$, large enough to insure a turbulent flow at this and

larger scales. Turbulence efficiently mixes the fluids in the annihilation zone, but does not significantly retard their mean motion in the depletion zone. Thus turbulence drives the flow to the solution we have discussed, wherein the annihilation rate is determined solely by the rate at which material can be transported toward the annihilation zone.

The drag on the fluid exerted by the CBR and the velocity redshift due to expansion suppress turbulence on large scales. The first effect dominates during the redshift range of interest, suppressing turbulence for scales $\lambda > v\, m_p\, c/(\sigma_T\, u_\gamma)$, which is larger than the width A of the annihilation domain.
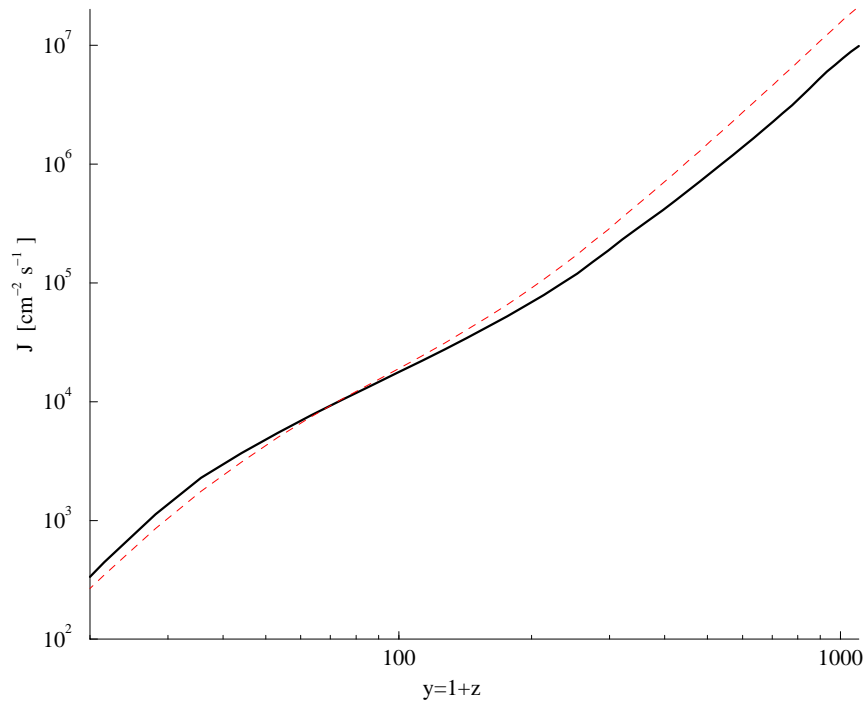

Figure 3: Annihilation rate J (in particles per cm^2 per second) as a function of redshift y. The solid curve is our numerical solution; the dashed curve is an approximate result discussed in the text.

4 Distortion of the CBR

Measurements of the CBR, being much more precise than those of the CDG, might be expected to provide the most stringent constraint on the $B = 0$ universe. In this section, we use our conservative calculation of the annihilation rate to estimate the distortion of the CBR spectrum. In performing this calculation, we make several approximations that somewhat overestimate the effect. Nonetheless, the consequent distortion lies well below the observed limit, and provides no constraint at all.

Annihilation produces relativistic electrons and energetic photons. Annihilation electrons have a direct effect on the CBR by scattering photons to higher energies, thereby skewing the CBR spectrum. Moreover these electrons heat the ambient plasma. The heated plasma produces an additional indirect spectral distortion. (The energetic photons from neutral pion decay have energies too high to have much effect on the cosmic microwave background.)

To compute the direct effect, we must determine the number of CBR photons scattered from energy ω_i to ω_f by a single electron. This function, $d^2 N(\omega_f, \omega_i)/d\omega_f \, d\omega_i$, is computed in Appendix A.2. The electron multiplicity per $p\bar{p}$ annihilation is similar to the photon multiplicity, measured [20] to be $\bar{g} \simeq 3.8$. The number of annihilation electrons made per unit volume and time is $\bar{g} \, J/d$, where $1/d \equiv y/d_0$ is the average domain surface-to-volume ratio at epoch y. The spectral distortion $\delta u_\gamma(\omega)$ (energy per unit volume and energy) satisfies a transport equation:

$$\left(y \frac{\partial}{\partial y} + \omega \frac{\partial}{\partial \omega} - 3 \right) \delta u_\gamma(\omega, y) =$$

$$\frac{\omega \bar{g} \, J(y)}{H(y) \, d(y)} \int d\nu \left(\frac{d^2 N(\nu, \omega)}{d\nu d\omega} - \frac{d^2 N(\omega, \nu)}{d\nu d\omega} \right) \equiv A(\omega, y) . \tag{9}$$

We have ignored absorption of UV photons by neutral hydrogen because the $B = 0$ universe is largely ionized.

The direct contribution to the CBR distortion is the solution to Eq. (9) evaluated at the current epoch: $\delta u_\gamma(\omega) \equiv \delta u_\gamma(\omega, 1)$. It is given by:

$$\delta u_\gamma(\omega) = \int_{y_R}^{y_S} \frac{dy}{y^4} \, A(\omega \, y, y) , \tag{10}$$

where we have confined the source to $1100 > y > 20$, the era of unavoidable annihilation. To evaluate the integral we use the annihilation rate J com-

puted in Section 3. Figure 4 displays the result for a current domain size of 20 Mpc. Note that $|\delta u_\gamma(\omega)|$ is always less than 3×10^{-3} cm$^{-3} \simeq 1.8 \times 10^{-6}\, T_0^3$. The limit set by COBE–FIRAS [21] on rms departures from a thermal spectrum is $|\delta u_\gamma(\omega)| < 7.2 \times 10^{-6}\, T_0^3$ throughout the energy range $T_0 < \omega < 10\, T_0$. This upper limit is four times larger than our computed signal for the minimum domain size. Because larger domains yield proportionally smaller results, we obtain no constraint on the $B = 0$ universe.

The indirect contribution to the CBR distortion results from a temperature difference $T - T_\gamma$ between the heated ambient fluid and the CBR. It may be described by the Sunyaev–Zeldovich parameter Y [22]:

$$Y = \int \frac{\sigma_T\, n_e (T - T_\gamma)}{m_e c^2}\, dl \; , \tag{11}$$

where the integral is along the photon path $dl = -c\, dy/y\, H(y)$.

Within the electron range, collisions between annihilation electrons and the plasma result in a temperature profile $T(y)$ shown as the solid curve in Fig. 2. Outside the electron range, reheating is due to photons up-scattered by these electrons, resulting in the temperature profile shown as the dashed curve. CBR photons may have traversed regions of both types. To compute Y, we use the higher temperature profile (the one within the electron range). We thereby overestimate the signal. Our result is $Y \lesssim 9 \times 10^{-7}$, which is over an order of magnitude below the COBE–FIRAS limit [21] of $|Y| < 1.5 \times 10^{-5}$. We conclude[7] that current observations of the CBR spectrum yield no constraint on the $B = 0$ universe.

The energy spectrum of uplifted CBR photons shown in Fig. 4 extends into the visible, falling like $1/\sqrt{\omega}$. Most of the energy remaining from nuclear annihilation resides in this tail. Nevertheless, the diffuse intensity of the night sky is well above this level.

5 The Diffuse Gamma-Ray Spectrum

In this section, we use our conservative calculation of the annihilation rate to determine a lower bound to the CDG signal. We find that annihilation in a $B = 0$ universe produces far more γ-rays than are observed.

---

[7]An additional contribution to Y arises as CBR photons pass through transitional regions being re-ionized, but is two orders of magnitude smaller than the effect we discussed.
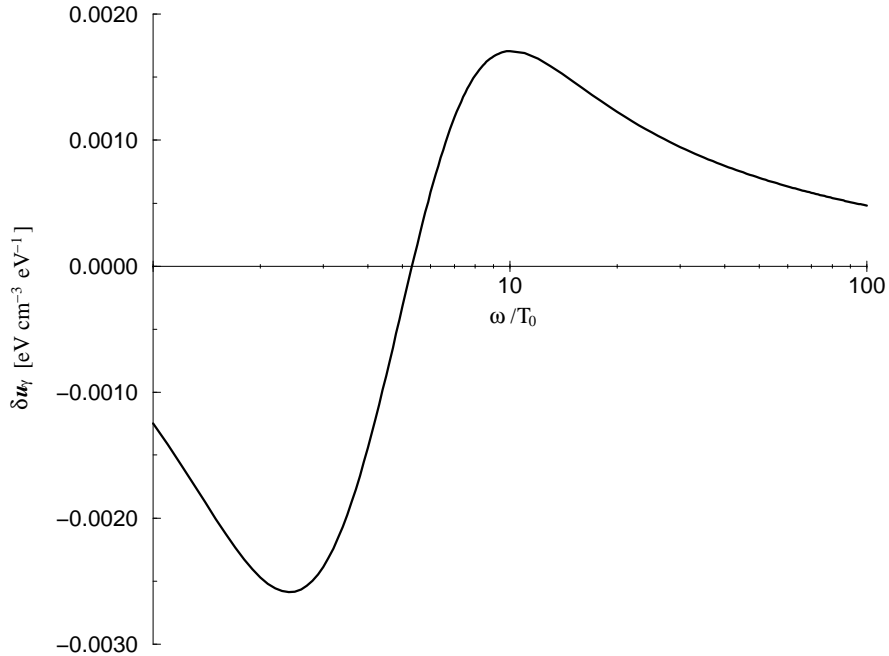
Figure 4: The CBR spectral distortion. Beyond the range shown, $\delta u_\gamma \propto 1/\sqrt{\omega}$, up to $\omega/T_0 \sim 10^4$.

The relic spectrum of γ-rays consists primarily of photons from π^0 decay. Let $\Phi(E)$ denote the inclusive photon spectrum in $p\bar{p}$ annihilation, normalized to $\bar{g}$, the mean photon multiplicity[8]. The average number of photons made per unit volume, time and energy is $\Phi(E)\,J/d$. These photons scatter and redshift, leading to a spectral flux of annihilation photons $F(E,y)$ (number per unit time, area, energy and steradian) satisfying the transport equation:

$$\left(y\,\frac{\partial}{\partial y} + E\,\frac{\partial}{\partial E} - 2\right) F(E,y) = -\frac{1}{H(y)}\,\Phi(E)\,\frac{c\,J}{4\,\pi\,d} + R(E,y)\;. \qquad (12)$$

[8]The measured photon spectrum can be found in [20] and is further discussed in Appendix A.

The first term on the RHS is the annihilation source and the second is a scattering sink. We slightly underestimate $F(E, y)$ by treating all scattered photons as effectively absorbed. In this case:

$$R(E, y) = \frac{c\,\sigma_\gamma(E)\,n_e(y)}{H(y)}\,F(E, y) \equiv g(E, y)\,F(E, y)\,, \qquad (13)$$

with σ_γ the photon interaction cross section and $n_e(y)$ the electron density. For the relevant photon energies, it matters little whether photons encounter bound or unbound electrons.

Integration of Eqs. (12)–(13) gives the photon flux today, $F(E) \equiv F(E, 1)$:

$$F(E) = \int_{y_S}^{y_R} \frac{c\,J(y')\,\Phi(Ey')}{4\pi\,d(y')}\,\exp\left[-\int_1^{y'} \frac{dy''}{y''}\,g(Ey'', y'')\right]\frac{dy'}{H(y')\,y'^3}\,. \qquad (14)$$

Measurements of the CDG flux are shown in Fig. 5. From 2 MeV to 10 MeV, preliminary COMPTEL satellite measurements [23] lie roughly an order of magnitude below[9] the earlier balloon data [24]. Figure 5 also shows our computed signal $F(E)$. The upper curve corresponds to the smallest allowed domains, $d_0 = 20$ Mpc, the lower curve to $d_0 = 1000$ Mpc. The signal is linear in $1/d_0$. The relic photon distribution is redshifted from the production spectrum (which peaks at $E \sim 70$ MeV), and is slightly depleted at low energies by attenuation.

Our conservative lower limit to the γ-ray signal conflicts with observations by several orders of magnitude and over a wide range of energies, for all values of $d_0 \lesssim 10^3$ Mpc, comparable to the size of the universe. We could argue that the satellite data excludes even larger domain sizes, but we would soon run into questions of the precise geometry and location of these nearly horizon-sized domains.

6   Closing Loopholes

Can our 'no-go theorem' for the $B = 0$ universe be skirted by changing the input parameters, modifying our hypotheses, or including other effects? Here we examine the sensitivity of our conclusions to the chosen values of cosmological parameters, to the possible existence of primordial magnetic fields, and to the assumed isentropic nature of primordial density fluctuations.

---

[9]This discrepancy is attributed by the authors of [23] to a rigidity-dependent background correction that the balloon experiments could not perform.
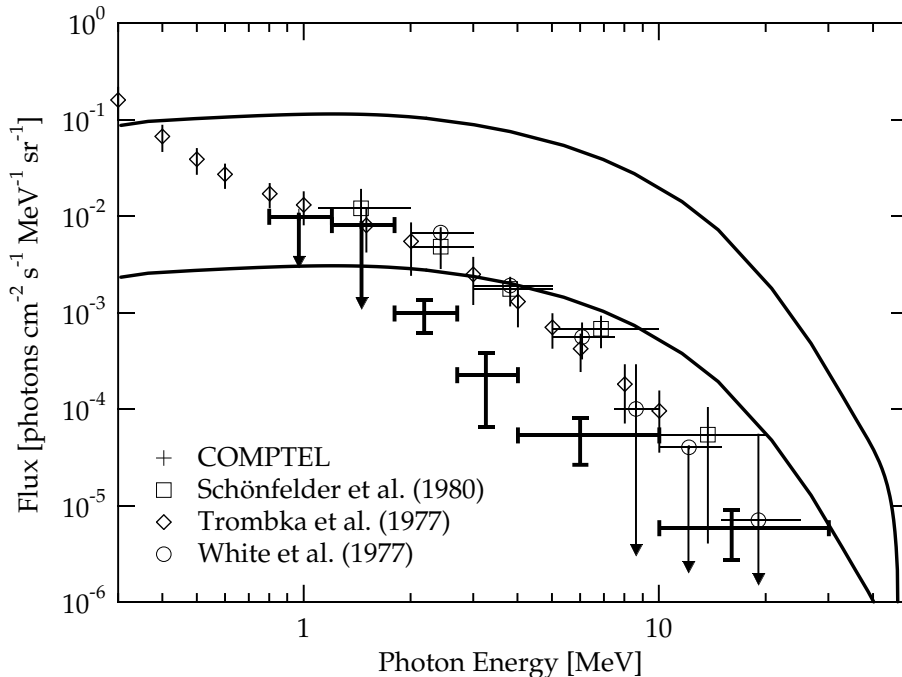
Figure 5: Data [23] and expectations for the diffuse γ-ray spectrum.

We used a flat and dark-matter-dominated universe with vanishing cosmological constant. For this case, the expansion rate is given by the simple expression $H(y) = y^{3/2} H_0$, with H_0 the Hubble constant. Other choices for the cosmological parameters ($\Omega_m \neq 1$ and/or $\Omega_\Lambda \neq 0$) would alter the y dependence of $H(y)$ as follows:

$$\frac{dy}{y} = -H(y)\,dt = -H_0 \left[(1 - \Omega)\,y^2 + \Omega_m\,y^3 + \Omega_\Lambda\right]^{1/2} dt \ . \qquad (15)$$

It is only through the modification of $H(y)$ that H_0, Ω_m and Ω_Λ affect our results.

We have recomputed the diffuse gamma background (CDG) for a range of observationally viable values of the cosmological parameters and are unable to suppress the signal by more than a factor of 2. The reason is easily seen. Equation (12) shows that $J \propto 1/H(y)$, and Eq. (14) shows that the CDG flux is proportional to $J/H(y)$, and hence to $H(y)^{-2}$. To suppress the flux, we must increase $H(y)$ beyond its value at $\Omega_m = 1$, $\Omega_\Lambda = 0$ and $h = 0.75$. No sensible value of Ω_Λ has much effect at $y \sim 20$, when most of the CDG

18

flux arises. For $\Omega_m = 2$ or $h = 0.5$, two borderline possibilities, the CDG flux would be reduced by about a factor of two, not altering our conclusions.

We assumed that electrons produced by annihilations travel in straight lines. This would not be true were there primordial (or magnetohydrodynamically generated) magnetic fields in the vicinity of domain boundaries. Fields with sufficiently short correlation lengths and large amplitudes would reduce the electron range. If the magnetically-reduced range still exceeds D, the width of the depletion zone, the annihilation rate is increased and our conclusions are strengthened. If the electron range were less than D, electrons would deposit their energy near the annihilation zone rather than throughout the plasma. However, heating by UV photons alone results in the temperature profile plotted in Fig. 2. Because $J \sim \sqrt{T}$, the CDG signal cannot be reduced by more than a factor of 3 relative to our previous results. Thus, the existence of magnetic fields at or after recombination cannot alter our conclusion.

Finally, we claimed that matter and antimatter domains must touch by recombination, if they are not to produce observable (and unobserved) scars in the CBR. Our argument depended on the absence of strictly isothermal fluctuations at recombination. If this hypothesis is false, matter and antimatter islands could be separated by regions of vanishing baryon density, with a uniform photon distribution throughout. If these isothermal voids are so wide that they persist after recombination, annihilation might be prevented. Annihilation might also be prevented by 'wrapping' different regions with domain walls, whose properties are designed to block the penetration of thermal matter while avoiding cosmological constraints [25]. We have not further pursued these contrived lines of thought.

7 Conclusions

Neither the notion of a universe containing islands of antimatter, nor the exploration of its observable consequences are new. Indeed, the literature includes diametrically opposed views as to the viability of such models. The purpose of this paper is to present a class of models (arguably, the most general) for which the observable universe consists of comparable numbers of domains containing either matter or antimatter. These models are parameterized by the typical domain size today, d_0. Direct searches for annihilation radiation show that $d_0 > 20$ Mpc, and future searches for antimatter among

cosmic rays may increase this lower bound by an order of magnitude.

We have found constraints on a matter–antimatter universe arising from phenomena taking place at cosmological distances. The potentially observable signals are identified as a distortion of the CBR, and the production of a relic flux of diffuse gamma-rays (CDG). We have computed these signals with conservative assumptions and considerations based on empirical evidence, but with as little theoretical prejudice as possible. We find that matter–antimatter encounters at domain boundaries are unavoidable from recombination to the onset of structure formation. The detailed dynamics underlying our calculation of the annihilation rate is complicated. The flow of matter into antimatter (and vice versa) is diffusive at large y and hydrodynamic at low y. Furthermore, energy deposition by the annihilation debris plays a crucial role, increasing the annihilation rate by up to two orders of magnitude relative to what it would have been if this effect had been neglected.

Part of the energy released by annihilations at cosmological distances ends up as microwave photons that would appear as a non-thermal correction to the cosmic background spectrum. However, we find that measurements of the CBR spectrum do not lead to a competitive constraint on the $B = 0$ universe.

High-energy photons produced by annihilations at cosmological distances (most of which survive to the current epoch) are redshifted to current energies of order 1 MeV, thereby contributing to the diffuse γ-ray spectrum. Our conservative estimate of the relic CDG flux far exceeds its measured value. Thus, we have ruled out a $B = 0$ universe with domains smaller than a size comparable to that of the visible universe[10]. It follows that the detection of $Z > 1$ antinuclei among cosmic rays would shatter our current understanding of cosmology, or reveal something unforeseen in the realm of astrophysical objects.

Acknowledgements

---

[10]Of course, it is not possible to exclude the existence of small and distant pockets of antimatter [26].

A   The Annihilation Debris

Each $p\bar{p}$ annihilation produces $\bar{g} \simeq 3.8$ electrons and positrons, and a similar number of photons. The photon spectrum has been well measured [20] and may be used to infer the electron spectrum. The photon distribution peaks at $E_\gamma \simeq 70$ MeV, and the average photon energy is $\langle E_\gamma \rangle \simeq 180$ MeV. The mean pion energy is twice that of the photon. About $1/4$ of the energy of a charged pion finds its way to an electron. (The muon retains $\sim 3/4$ of the charged-pion energy, of which $\sim 1/3$ passes to the decay electron.) Thus, we expect an electron spectrum peaking at $E_e \sim 35$ MeV with $\langle E_e \rangle \sim 90$ MeV.

We must determine various properties of an annihilation electron in the redshift interval $20 < y < 1100$: its mean range, its effect on the CBR, the energy it deposits in matter along its trajectory, and the ionizing effect of its passage. Three mechanisms control the electrons' motion in the fully ionized plasma. With $p = \beta \gamma m_e$ and in terms of our fiducial cosmological parameters, they are:

- Cosmological redshift:

$$-\left.\frac{dp}{dt}\right|_C = \frac{\dot{R}}{R}p = H_0\, p\, y^{3/2} = K_C(y)\,\beta\gamma\,, \qquad (16)$$

$$K_C(y) = 1.3 \times 10^2\, y^{3/2}\, \frac{\text{eV}}{\text{Mpc}}\,.$$

- Collisions with CBR photons:

$$-\left.\frac{dp}{dt}\right|_\gamma = \frac{4\,\pi^2}{45}\, \sigma_T\, T_\gamma^4\, \frac{E^2}{m_e^2}\, \beta = K_\gamma(y)\,\beta\gamma^2\,. \qquad (17)$$

$$K_\gamma(y) \simeq 0.7\, y^4\, \frac{\text{eV}}{\text{Mpc}}\,.$$

- Collisions with ambient plasma electrons:

$$-\left.\frac{dp}{dt}\right|_M \simeq 2\pi\, n_e\, \frac{\alpha^2}{m_e\beta^2}\, \ln\left(\frac{m_e^3\,\beta^2}{16\,\pi\, n_e\, \alpha}\right) \simeq K_M(y)\, \frac{n_e}{n_\infty}\, \frac{1}{\beta^2} \quad (18)$$

$$K_M(y) \simeq 5.5\, y^3\, \frac{\text{eV}}{\text{Mpc}}\,.$$

where n_e is the position-dependent electron number density while n_∞ is its value far enough from a domain boundary to be unaffected by annihilation and fluid motion.

A.1   The Range of Annihilation Electrons

Annihilation electrons lose energy as they redshift, but this mechanism—given by Eq. (16)—is negligible compared with collisional energy loss throughout the interval $20 < y < 1100$. Collisions with CBR photons—given by Eq. (17), for which $dp/dt \propto \gamma^2$—dominate over most of the trajectory. As an electron becomes non-relativistic, collisions with background electrons—given by Eq. (18), for which $dp/dt \propto 1/\beta^2$—come into play. These mechanisms cross over at $\beta^3 \gamma^2 \simeq 8/y$, a point denoted by β_{eq} (γ_{eq}). Some typical values are $\beta_{eq} \simeq 0.62$, 0.33, 0.19 at $y = 20$, 200, 1100.

To compute the range $L(\gamma_0, y)$ of an electron with initial energy $\gamma_0 m_e$, we use Eq. (17) throughout its trajectory, and ignore the small effect of multiple-scattering corrections. For $y \gtrsim 20$ the neglect of other energy-loss mechanisms leads to a negligible overestimate of L. Integrating Eq. (17), we find:

$$L(\gamma_0, y) = \frac{m_e}{K_\gamma} \arcsin \beta_0 \simeq 0.8 \times 10^{-6} \left(\frac{y_R}{y} \right)^4 \ \text{Mpc}. \tag{19}$$

For an initially relativistic electron $\arcsin \beta_0 \simeq \pi/2$, and the electron range is insensitive to the initial electron energy. The dependence of L on γ_0 is hereafter suppressed.

The previously established limit on domains of uniform composition is $d(y) \gtrsim 20/y$ Mpc. For $y < 30$, the electron range exceeds this minimal size and our one-dimensional approximation breaks down. Because we find a much stronger limit on the minimal domain size, this complication need not be faced. The result for the electron range, including all three sources of energy loss Eqs. (17)–(19), is plotted in Fig. 1. Throughout the relevant redshift interval, L is small compared with the horizon.

A.2   UV Photons

We compute the spectral distortion caused by the passage of one electron (with initial energy $E_0 = \gamma_0 m_e$) through a thermal bath of CBR photons. Compton scatterings conserve photon number but skew the spectrum toward

higher energies. The initial spectral distribution of CBR photons is $dn_\gamma/d\omega = (\omega/\pi)^2\mathcal{N}(\omega)$, with $\mathcal{N} = 1/(e^{\omega/T_\gamma} - 1)$. Let $d^2N(\omega_f, \omega_i)/d\omega_i\, d\omega_f$ denote the number of photons transferred by one electron from the frequency interval $d\omega_i$ to the interval $d\omega_f$. Define:

$$\frac{d^2N(\omega_f, \omega_i)}{d\omega_i\, d\omega_f} = \frac{d^2N(\omega_f, \omega_i)}{d\omega_f\, dn}\, \frac{dn_\gamma(\omega_i)}{d\omega_i} \ . \tag{20}$$

The function $d^2N(\omega_f, \omega_i)/d\omega_f\, dn$ may be regarded as the spectral distribution of struck photons of frequency ω_f produced during the voyage of one energetic electron through an isotropic, monochromatic photon gas of unit density and frequency ω_i.

Let $d\Omega_i(\theta_i, \phi_i)$ be the differential solid angle about the initial photon direction, and v_i be the relative speed of the colliding particles. We choose to measure angles relative to the total momentum direction of the colliding particles. The function $d^2N/d\omega_f\, dn$ is obtained by averaging the differential transition rate over target photon directions, and integrating in time, along the electron trajectory:

$$\frac{d^2N}{d\omega_f\, dn} = \int dt \int \frac{d\Omega_i}{4\pi} v_i \frac{d\sigma}{d\omega_f} \ , \tag{21}$$

where we have neglected the small effect of stimulated emission.

The computation is simplified if we note that $\gamma T_\gamma \ll m_e$, so that the Thompson limit applies and

$$v_i \frac{d\sigma}{d\omega_f} = \frac{3\sigma_T}{16\mu^4\beta^5\gamma^{10}\omega_i} \Big\{ \mu^2\gamma^2\,(1 + 2\gamma^2)(1 - 2\gamma^2\mu) + (3 - 4\gamma^2)\mu^4\gamma^4 + 4\mu^6\gamma^6$$
$$+ r\,(r - 2\,\mu\,\gamma^2)\,\big[3 - 6\,\mu\,\gamma^2 + \mu^2\gamma^2\,\big(1 + 2\,\gamma^2\big)\big] \Big\} \Theta(\frac{\mu}{1 + \beta} < r < \frac{\mu}{1 - \beta}) \ ,$$

where $r \equiv \omega_f/\omega_i$ and $\mu \equiv 1 - \beta\cos\theta_i$.

Carrying out the integrations in Eq. (21) gives our result for $d^2N/d\omega_f\, dn$. (The dt integration is most easily performed by trading dt for dp using Eq. (17). This integral extends from from $p_0 \simeq m_e\,\gamma_0$ to $p_{eq} \simeq m_e\,\gamma_{eq}\,\beta_{eq}$. The result is insensitive to the y-dependence of p_f.)

A.3   Ionization

Here we show that the fluid is almost totally ionized by annihilation electrons at all relevant times. The value of the ionization fraction, x, results from a

compromise between the recombination and ionization rates. Annihilation electrons ionize the material they traverse both directly, via electron-atom collisions as described by Eq.(18), or indirectly, via the UV showers discussed in Appendix A.2. We discuss the latter effect, which is more important.

Many of the photons up-scattered by annihilation electrons have energies exceeding the hydrogen binding energy ($B = 13.6$ eV), and can ionize hydrogen atoms via $\gamma + H \rightarrow e + p$. The photoionization cross section for hydrogen atoms in their ground state, σ_K, falls rapidly from a very large threshold value $\sigma_K(B) \simeq 8 \times 10^{-18}$ cm^2:

$$\sigma_K(\omega) \simeq \sigma_K(B) \, (B/\omega)^3 \, \Theta(\omega - B) \; . \tag{22}$$

We compute the effective ionization cross section $\bar{\sigma}_K$ for the entire UV shower associated with a single electron by integrating the product of σ_K with the photon number distribution:

$$\bar{\sigma}_K \equiv \int \frac{d^2 N}{d\omega_i \, d\omega_f} \, \sigma_K(\omega_f) \, d\omega_f \, d\omega_i \simeq 1.4 \times 10^{-13} \text{ cm}^2 \, \sqrt{1100/y} \; . \tag{23}$$

This cross section is four orders of magnitude larger than $\sigma_K(B)$ and reflects the large number of photons scattered by a single electron.

The total ionization rate is the difference of the photonionization rate and the recombination rate. The former is obtained by multiplying the effective ionization cross section for a single annihilation electron $\bar{\sigma}_K$ by the flux of electrons. Because half of the $e^\pm$ produced in an annihilation zone move to either side, the flux is half the multiplicity $\bar{g}$ times the annihilation rate J. The total ionization rate $\dot{x}$ (per second and per baryon) is:

$$\dot{x} = \frac{\bar{g}}{2} \, J \, (1 - x) \, \bar{\sigma}_K - n_e \, x^2 \, \langle \sigma_{\text{rec}} \, v_e \rangle \; , \tag{24}$$

where the recombination coefficient to all states but the ground state is

$$\langle \sigma_{\text{rec}} \, v_e \rangle \simeq 1.14 \times 10^{-13} \, T^{-1/2} \left[1 - 2.20 \log T + 0.814 \, T^{1/3} \right] \text{ cm}^3 \, \text{s}^{-1} \; . \tag{25}$$

The coefficient of $1 - x$ in Eq. (24) is much greater than the coefficient of x^2 at all relevant epochs. Consequently, the ionization is very close to one:

$$1 - x \simeq \frac{2 \, n_e \langle \sigma_{\text{rec}} \, v_e \rangle}{\bar{g} \, J \, \bar{\sigma}_K} \ll 1 \; . \tag{26}$$

24

In the previous argument, no allowance was made for photon absorption despite the large photoionization cross section. Because the (quasi-)equilibrium ionization is nearly total, UV photons are unlikely to encounter atoms.

Near the region of electron production, the UV photon shower has not fully developed, so that the ionization is smaller than Eq. (26) indicates. Our calculation of $dN/d\omega_f dn$ can be modified to treat this case. We find that the UV flux near the annihilation zone is sufficient to maintain total ionization to within a few percent.

The UV flux generated by annihilation is sufficient to prevent recombination by producing and sustaining almost total ionization. However, for large values of d_0, regions lying far from domain boundaries recombine as in a standard cosmology. A moving front develops between ionized and recombined regions as the UV flux progresses. The velocity of the front is

$$v_f \sim \frac{c}{1 + \xi} ,$$

where ξ is the ratio of the nucleon number density to that of the incident UV flux. We find $v_f \sim c/3$ at $y = 1100$ and $v_f \sim c$ at $y = 20$. The intense energy deposition taking place within the front makes an unobservably small contribution to the Sunyaev–Zeldovich parameter.

A.4 Energy Deposition

We compute the heat function H_ϵ: the energy deposited in the plasma, per unit volume and time, by annihilation electrons and UV photons.

In regions within the electron range, this function is dominated by the primary electron contribution. For $\gamma > \gamma_{eq}$, collisions with CBR photons determine the evolution of the electron velocity according to Eq. (17). Denoting the energy deposition to matter for this portion of the trajectory by $\mathcal{E}_1$, we integrate Eq. (18) to find:

$$\mathcal{E}_1 = K_M(y) \frac{n}{n_\infty} \int_0^{L'} \frac{dx}{\beta^2} = \frac{K_M}{K_\gamma} \frac{m_e c^2}{\beta_{eq} \gamma_{eq}} \frac{n}{n_\infty} . \qquad (27)$$

Here L' is the distance traveled when $\gamma = \gamma_{eq}$:

$$L'(y) = (m_e/K_\gamma) \arccos \beta_{eq} . \qquad (28)$$

Most of the remaining energy, $\mathcal{E}_2 \simeq (\gamma_{eq} - 1) m_e c^2$, is deposited in matter over a relatively small distance interval. About one third of the energy deposition to matter takes place during this short stopping stage. In the following

analysis, we ignore this term, thereby underestimating electron heating by $\sim 30\%$, and slightly underestimating the production of CDG photons.

Electrons arise as an isotropic flux from the thin annihilation zone of width A. The angular average, per electron, of the energy deposition to matter at a distance $l \gg A$ from this zone is:

$$-\left\langle \frac{dE}{dl} \right\rangle_M \simeq \int_{l+A}^{L'} \frac{dx}{x} \left[K_M(y) \frac{n}{n_\infty} \frac{1}{\beta^2} \right] , \qquad (29)$$

where the integration variable is the distance traveled by an electron along its trajectory. Within the depletion zone $\langle dE/dl \rangle_M$ is a slowly-varying function of l that is roughly proportional to the electron density n_e:

$$\left\langle \frac{dE}{dl} \right\rangle_M \simeq a \; y^3 \; \frac{\text{eV}}{\text{Mpc}} , \qquad (30)$$

where $10 \lesssim a \lesssim 20$. For our computations we use the smallest value of a.

Half of the $e^\pm$ produced in an annihilation zone move to either side. Thus the $e^\pm$ flux is $\bar{g} \, J/2$, and the electron contribution to the heat function is:

$$H_\epsilon = -\frac{\bar{g}}{2} \, J \left\langle \frac{d\,E}{dl} \right\rangle_M . \qquad (31)$$

The UV photon contribution is small in comparison with that of the electrons.

Outside the electron range, only UV photons contribute to H_ϵ. In an ionizing collision, $\gamma + H \rightarrow e + p$, the mean kinetic energy δE of the recoiling photoelectron is:

$$\delta \, E = \frac{1}{\bar{\sigma}_K} \int \omega \, \frac{d^2 N}{d\omega \, d\omega_i} \, \sigma_K(\omega) \, d\omega \, d\omega_i - B \simeq 5.4 \text{ eV} , \qquad (32)$$

where the cross sections and distribution function are those of Appendix A.2. The rate per unit volume of such collisions is $J \bar{\sigma}_K (1-x) n_e \bar{g}/2$. Using Eq. (26) we express this rate as $n_e^2 \langle \sigma_{\text{rec}} v_e \rangle$. Multiplying by the mean recoil energy, we obtain the heat function:

$$H_\epsilon = \delta E \, \langle \sigma_{\text{rec}} v_e \rangle \, n_e^2 . \qquad (33)$$

The UV photon flux has disappeared from this expression, reflecting the quasi-equilibrium state of the ionization. As a welcome consequence, H_ϵ is insensitive to additional UV photons arising from annihilation zones other than the nearest.

References

[1] *The Astromag Project.* See, for instance, J.F. Ormes and R.E. Streitmatter, NASA report 91-047; *The Magnetic Spectrometer PAMELA,* O. Adriani *et al.*, WIZARD Collaboration, LNF-95-051-PF Report (1995) 23, Presented at 24th International Cosmic Rays Conference, Rome, Italy, 1995.

[2] S.P. Ahlen *et al.,* N.I.M. **A350** (1994) 351.

[3] *The Alpha Matter Spectrometer*, MIT, 1995.

[4] S.P. Ahlen *et al.*, Ap. J. **260** (1982) 20.

[5] G. Steigman, Annu. Rev. Astr. Ap. **14** (1976) 339.

[6] F.W. Stecker, D.L. Morgan and J. Bredekamp, Phys. Rev. Lett. **27** (1971) 1469; F.W. Stecker, Nucl. Phys. **B252** (1985) 25; A.K. Mohanty and F.W. Stecker, Phys. Lett. **143B** (1984) 351; Y.T. Gao, F.W. Stecker, M. Gleiser and D.B. Cline, Ap. J. **L37** (1990) 361.

[7] R. Omnès, Phys. Rep. **C3** (1970) 1. For a recent review, see A.D. Dolgov, Hyperfine Interactions **76** (1993) 17.

[8] A. Dudarewicz and A.W. Wolfendale, Mon. Not. R. Astron. Soc. **268** (1994) 609.

[9] A. Sakharov, JETP Lett. **5** (1967) 24.

[10] A.G. Cohen, A. De Rújula and M.B. Gavela, unpublished.

[11] For a recent discussion, see N. Hata, G. Steigman, S. Bludman and P. Langacker, `astro-ph/9603087`.

[12] R. Sachs and A. Wolfe, Astrophys. J. **147** (1967) 73.

[13] J. Silk, Ap. J. **151** (1968) 459.

[14] P. J. E. Peebles, *Principles of Physical Cosmology,* Princeton University Press (1993), 611.

[15] *Ibid.,* p. 680.

[16] See for instance S. Weinberg, *Gravitation and Cosmology: Principles and Applications of the General Theory of Relativity*, Wiley (1972).

[17] D.L. Morgan and V.W. Hughes, Phys. Rev. **D2** (1970) 1389.

[18] W.H. Kinney, E.W. Kolb and M.S. Turner, `astro-ph/9704070`.

[19] L.D. Landau and E.M. Lifshitz, *Fluid Mechanics*, Pergamon Press (1959).

[20] L. Adiels *et al.*, Phys. Lett. **B182** (1986) 405; S. Ahmad *et al.*, Phys. Lett. **152** (1985) 135.

[21] D.J. Fixsen, E.S. Cheng, J.M. Gales, J.C. Mather, R.A. Shafer and E.L. Wright, `astro-ph/9605054`.

[22] Ya.B. Zeldovich and R.A. Sunyaev, Ap. Space Sci. **4** (1969) 301.

[23] S.C. Kappadath *et al.*, Proc. 12th Int. Cosmic Ray Conf. **25** (1995) Vol. 2; S.G. Kappadath *et al.*,

`ftp://unhgro.unh.edu/pub/papers/kappadath_cdg_24icrc.ps.gz`.

[24] C.E. Fichtel *et al.*, Ap. J. **198** (1975) 163; E.P. Mazets *et al.*, Astrophysics and Space Science **33** (1975) 347; J.I. Trombka *et al.*, Ap. J. **212** (1977) 925; V. Schonfelder *et al.*, Ap. J. **240** (1980) 350; V. Schonfelder *et al.* Ap. J. Supp. **86** (1993) 657; R.S. White *et al.*, Ap. J. **218** (1977) 920.

[25] Ya. B. Zeldovich, I. Yu. Kobzarev and L. B. Okun, Sov. Phys. JETP **40** (1974) 1.

[26] A.D. Dolgov and J. Silk, Phys. Rev. **D47** (1993) 4244.